Magneto-optical study on excitonic spectra in $(C_6H_{13}NH_3)_2PbI_4$

Takeshi Kataoka, Takashi Kondo, and Ryoichi Ito

Department of Applied Physics, Faculty of Engineering, The University of Tokyo, 7-3-1 Hongo, Bunkyo-ku, Tokyo 113, Japan

Satoshi Sasaki, Kazuhito Uchida, and Noboru Miura

Institute for Solid State Physics, The University of Tokyo, 7-22-1 Roppongi, Minato-ku, Tokyo 106, Japan

(Received 30 April 1992; revised manuscript received 8 September 1992)

Magnetoabsorption spectra of the lowest-energy excitons in a layered perovskite-type material $(C_6H_{13}NH_3)_2PbI_4$ have been measured under pulsed high magnetic fields up to 42 T at 4.2 K in the Faraday configuration ($E \perp c \| B$) and the Voigt configuration ($E \perp c \perp B$). Energy shifts and splittings in the spectra for the Voigt configuration have been observed in this material. For the Faraday configuration, the Zeeman splitting with small diamagnetic shifts has clearly been detected. The diamagnetic coefficients obtained are much smaller than that for PbI_2, suggesting that the Wannier-exciton model is not a good approximation for the lowest-energy excitons in $(C_6H_{13}NH_3)_2PbI_4$. Theoretical analysis based on the cationic Frenkel-exciton model yields semiquantitative agreement with the experimental results.

I. INTRODUCTION

The layered perovskite-type materials $(C_nH_{2n+1}NH_3)_2PbI_4$ are natural quantum-well systems, in which excitons and charge carriers are tightly confined in monomolecular layers of $[PbI_4]$ sandwiched between organic barrier layers consisting of alkylammonium chains $[C_nH_{2n+1}NH_3]$. Owing to intrinsically flat well-barrier interfaces and very large band-gap energies of the barrier layers compared with those of the well layers, excitons in this group of materials may behave as ideal two-dimensional (2D) systems. In fact, it has been found that the lowest-energy excitons in $(C_nH_{2n+1}NH_3)_2PbI_4$ have an extremely large binding energy ($E_b = 300 \sim 500$ meV) and oscillator strength ($f \sim 0.7$ per formula unit).[1-4] Thus the excitons are so stable that the excitonic absorption peaks are clearly observable even at room temperature. Another unique feature of these materials is that the dielectric constant of the barrier layers is much smaller than that of the well materials. This has aroused interest in whether they are the rare systems in which one may observe the dielectric-confinement effect[5,6] where the effective Coulomb interaction of an electron and hole in the well layers is significantly enhanced.

In spite of some previous studies on the excitons in these materials,[1-4,7] their nature is still by no means clear. It is very interesting to know what the internal motions of the excitons having such a large binding energy and oscillator strength are like. In particular, there is an important question as to whether the excitons having such a large binding energy and oscillator strength can legitimately be described as Wannier excitons where the electron and hole bind weakly to each other and the effective-mass approximation is valid. Magneto-optical measurements under high magnetic fields should be highly useful in exploring this problem.

Magnetoabsorption (MA) spectra have recently been measured on $(C_{10}H_{21}NH_3)_2PbI_4$ at 4.2 K.[7] In this crystal, however, because of severe twinning and the resultant deterioration of the crystal quality due to structural phase transitions below room temperature, the absorption lines of the excitons became too broad at low temperatures to observe discernible changes in the Voigt configuration ($E \perp c \perp B$) and accurately determine the amount of the energy shift in the Faraday configuration ($E \perp c \| B$). Thus, a detailed investigation of the nature of the excitons has not been possible with $(C_{10}H_{21}NH_3)_2PbI_4$.

We have found that $(C_6H_{21}NH_3)_2PbI_4$, unlike $(C_{10}H_{21}NH_3)_2PbI_4$, undergoes no structural phase transition below room temperature, retaining its crystal quality down to very low temperatures. This results in $(C_6H_{13}NH_3)_2PbI_4$ having much sharper exciton lines than $(C_{10}H_{21}NH_3)_2PbI_4$, and makes it ideally suited to the study of the nature of the excitons.

In this paper we present the results of our magneto-optical study of the lowest-energy excitons in $(C_6H_{13}NH_3)_2PbI_4$. In Sec. II the sample preparation and the experimental procedure are briefly described. In Sec. III the results of the MA measurements are presented. In Sec. IV we discuss in detail the nature of the excitons on the basis of the experimental results. We analyze MA spectra by both the Wannier and Frenkel models and consider which is more suitable for this exciton system. Finally, the conclusion is given in Sec. V.

II. EXPERIMENTAL PROCEDURE

The samples used were polycrystalline films (~ 100 nm thick) which were spin-coated on 4-mm-diam quartz substrates. X-ray-diffraction study showed that the spin-coated films were highly oriented with the c axis perpendicular to the substrate surfaces. In the $k \| c$ configuration, the thin-film samples exhibit optical properties

almost identical to those of single-crystalline samples. This is because $(C_6H_{13}NH_3)_2PbI_4$ has very small anisotropy in the ab plane (layer plane), as has been confirmed by a crystal-structure analysis and the conoscopic figure measurements and polarized reflection spectra taken on single crystals.

The good quality of our samples can be seen by comparing the exciton absorption spectra at 4.2 K of $(C_{10}H_{21}NH_3)_2PbI_4$ and $(C_6H_{13}NH_3)_2PbI_4$, as shown in Fig. 1. The broad absorption line of $(C_{10}H_{21}NH_3)_2PbI_4$ is resolved in $(C_6H_{13}NH_3)_2PbI_4$ into four sharp lines and a relatively small high-energy line. The line splitting was also observed in the normal-incidence reflection spectrum from a single crystal, indicating that it is an intrinsic property of $(C_6H_{13}NH_3)_2PbI_4$. Since, as we will see in the following, all the lines behave quite similarly in magnetic fields, they probably involve the same electric transitions, not originating from different orbital states split by crystal fields or spin-orbit interaction. The multiple absorption lines may be phonon sidebands, though the tentative Raman data are not consistent with the magnitude of the line splitting.

MA spectra were measured at 4.2 K in pulsed magnetic fields up to 42 T in the Faraday configuration $(E \perp c \| B, k \| c)$ and the Voigt configuration $(E \perp c \perp B, k \| c)$.[8,9] The samples were immersed in liquid helium in a specially designed cryostat in which a coil made of Nb/Ti superconducting wires was installed in a liquid-nitrogen bath. Magnetic fields up to 42 T were generated by discharging a condenser bank into the coil. The light source was a flash xenon lamp. Light from the xenon lamp was introduced to the samples through an optical fiber and a polarizer. The light transmitted through the samples was guided through another fiber and a spectrometer to an optical multichannel analyzer (OMA) equipped with a diode-detector array. The xenon flash started at almost the same time the gate of the OMA was opened. MA spectra were taken while the gate of the OMA was open, for about 1 ms, when the magnetic field reached it peak value. The variation of the magnetic field during the measurements was less than 2%. Although the spectral resolution of the measurements was about 1.4 Å, it was possible to determine the amount of energy shifts with a much better resolution, about 0.25 Å, by curve fitting.

III. EXPERIMENTAL RESULTS

Figure 2 shows the MA spectra of the lowest-energy excitons in the Faraday configuration $(E \perp c \| B, k \| c)$ for the left-handed circular (σ^+) polarization. The MA spectrum for the right-handed (σ^-) polarization is displayed only for the highest magnetic field by a dashed line for comparison. The four absorption lines shift toward higher energies for the σ^+ polarization and toward lower energies for the σ^- polarization as the magnetic field is increased. The absorption strength of the lines
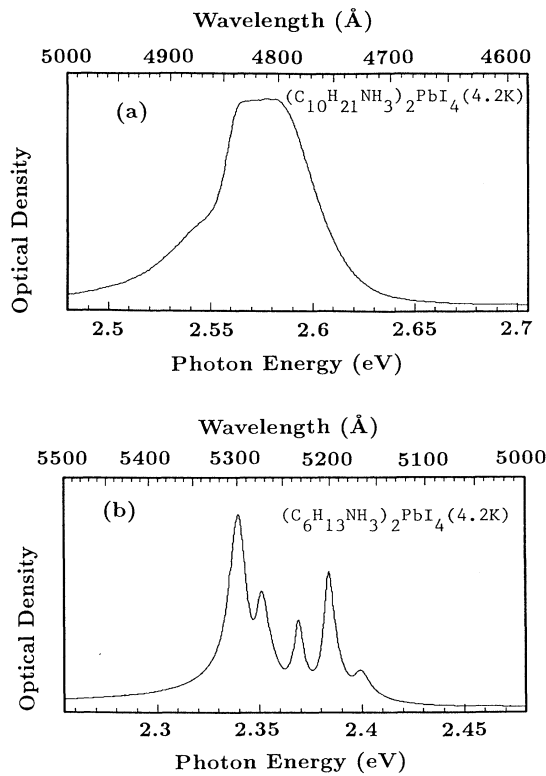

FIG. 1. Absorption spectra of the lowest exciton of the spin-coated highly oriented film of (a) $(C_{10}H_{21}NH_3)_2PbI_4$ and (b) $(C_6H_{13}NH_3)_2PbI_4$. Note that (a) is not saturated
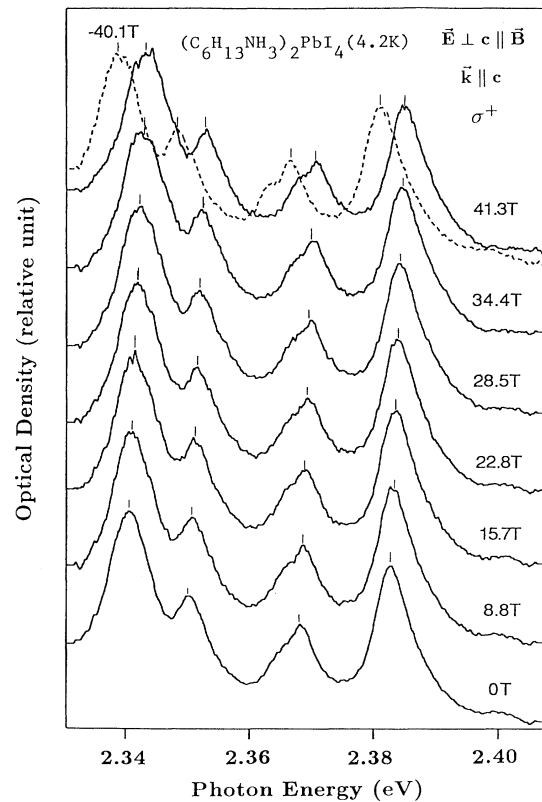

FIG. 2. MA spectra of $(C_6H_{13}NH_3)_2PbI_4$ in the Faraday configuration for the σ^+ polarization (solid lines) and the σ^- polarization (dashed line).

shows no change. Note that all the four lines exhibit almost the same shift. The peak energies of the absorption lines are plotted by open circles in Fig. 3 as a function of the magnetic field. The absorption lines are labeled in order of increasing energy. The Zeeman splitting with small diamagnetic shifts is clearly observed. The solid lines in Fig. 3 are theoretical curves fitted with the method of least squares by the well-known formula

$$E = E_0 \pm \tfrac{1}{2} g_\perp \mu_B B + c_0 B^2 , \qquad (1)$$

where E_0 is the energy of each absorption line at 0 T, $g_\perp$ the effective g factor perpendicular to the ab plane, c_0 the coefficient of the diamagnetic term, and μ_B the Bohr magneton. The second term in Eq. (1) is the Zeeman term and the third term represents the diamagnetic shift. The fitting is very satisfactory; it is indeed much better than that obtained with the previous MA measurements on $(C_{10}H_{21}NH_3)_2PbI_4$.[7] This is due to a much higher accuracy in determining the energy shifts of the narrower

TABLE I. The effective g factors $g_\perp$ and the diamagnetic coefficients c_0 obtained by the fitting at each excitonic absorption line in $(C_6H_{13}NH_3)_2PbI_4$ and those obtained by Nagamune, Takeyama and Miura (Ref. 10) in PbI_2.

	First line	Second line	Third line	Fourth line	PbI_2
$g_\perp$	1.80	1.81	1.70	1.61	0.89
c_0 $(10^{-7}$ eV/T$^2)$	3.53	3.12	2.70	2.16	9.7

lines in $(C_6H_{13}NH_3)_2PbI_4$ than in $(C_{10}H_{21}NH_3)_2PbI_4$. Table I shows $g_\perp$ and c_0 obtained by the above fitting for each absorption line and those for PbI_2 obtained by Nagamune, Takeyama, and Miura[10] for comparison. In $(C_6H_{13}NH_3)_2PbI_4$ the diamagnetic shifts are considerably smaller than those in PbI_2 and $g_\perp$ much larger. It is worth noting that the $g_\perp$ values of the four lines are almost the same, suggesting that the four lines probably belong to the same atomic orbitals.
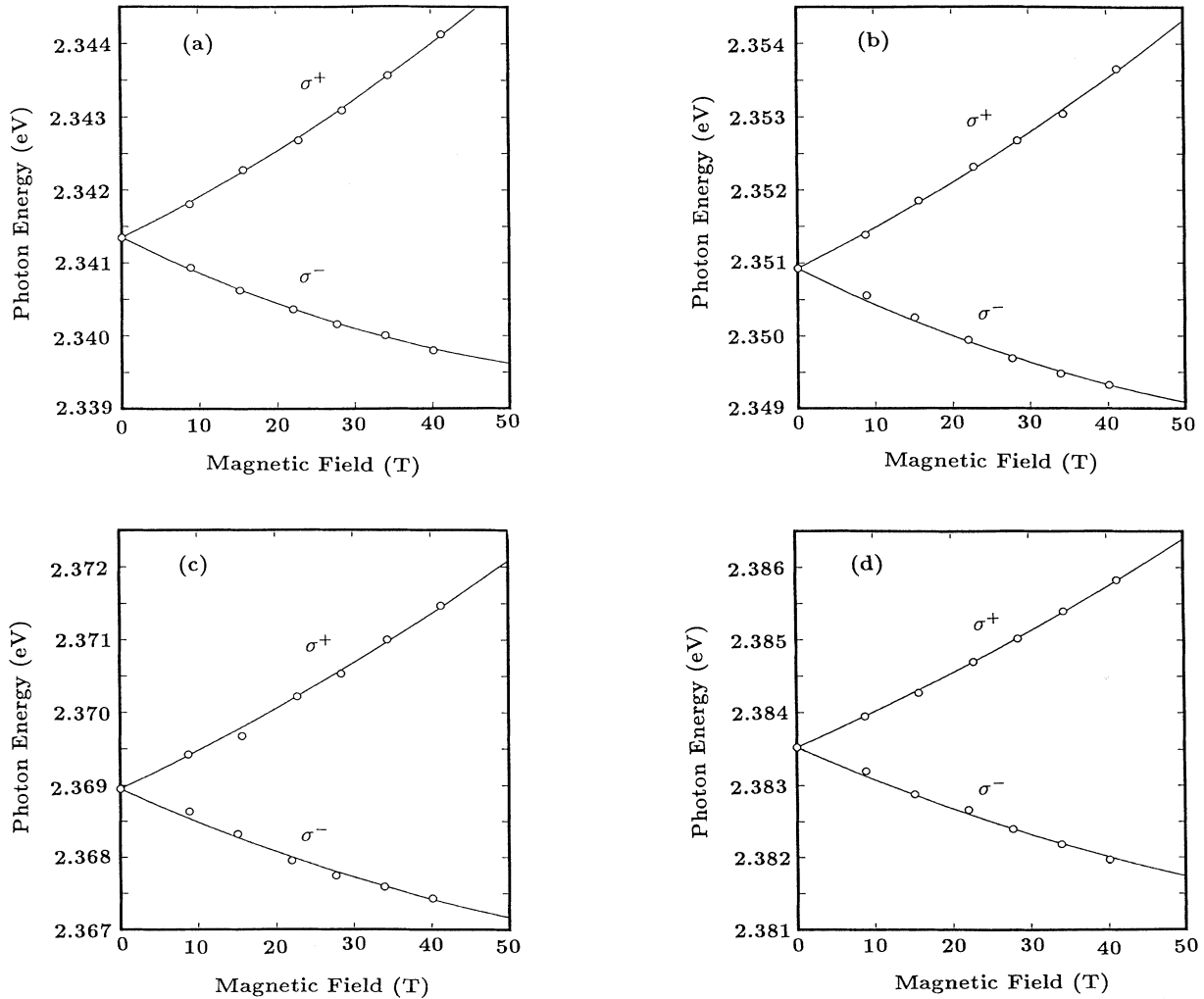

FIG. 3. Energy shift as a function of the magnetic field in the Faraday configuration for (a) the first line, (b) the second line, (c) the third line, and (d) the fourth line. Open circles represent the experimental results and solid lines show the theoretical fitting with the method of least squares.
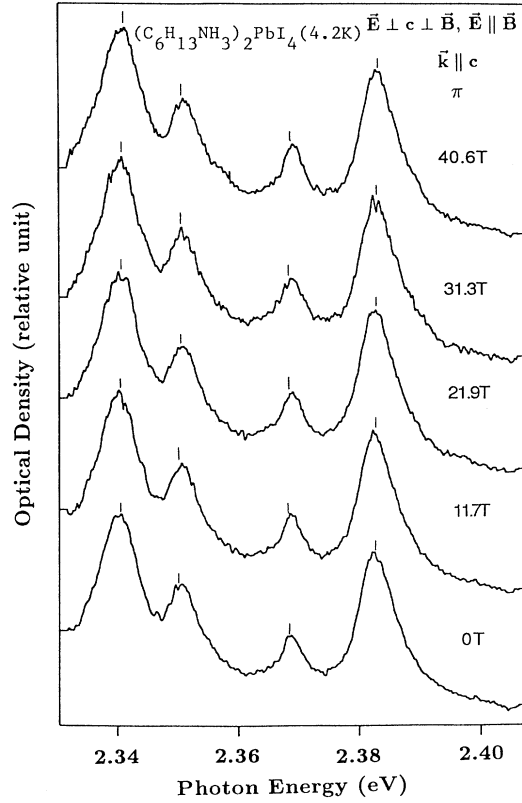
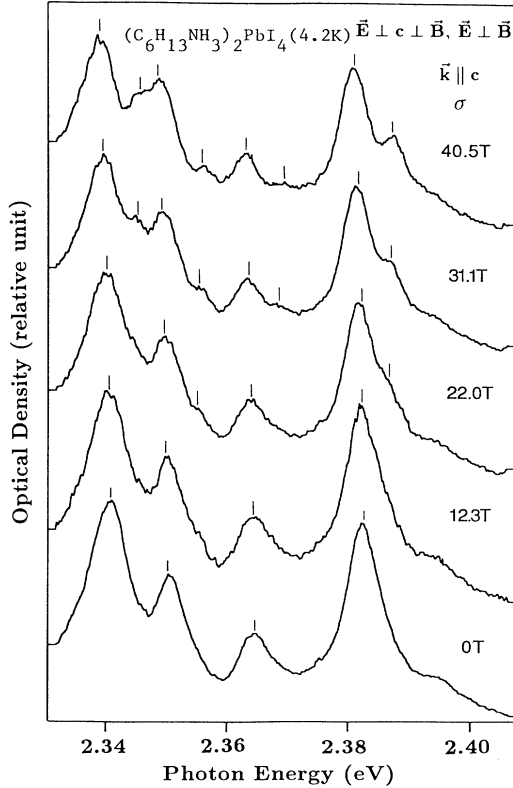FIG. 4. MA spectra in the Voigt configuration for the π polarization

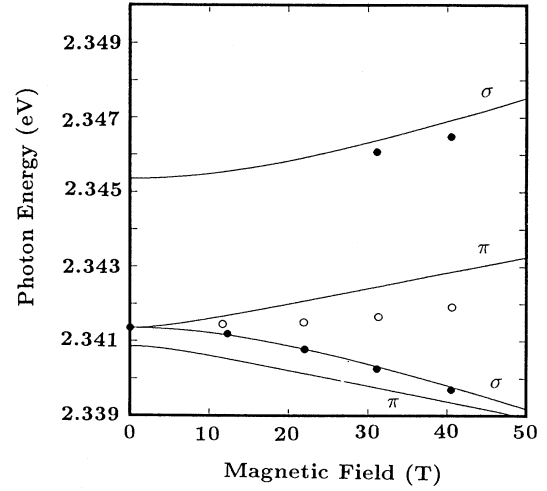FIG. 5. MA spectra in the Voigt configuration for the σ polarization.

FIG. 6. Energy shift and splitting of the first line as a function of the magnetic field in the Voigt configuration. Open circles are for the π polarization and closed circles for the σ polarization. The solid lines have been theoretically calculated based on the cationic Frenkel-exciton model.

Figures 4 and 5 show the MA spectra in the Voigt configuration for the π polarization $(\mathbf{E}\perp c\perp\mathbf{B}, \mathbf{E}\|\mathbf{B}, \mathbf{k}\|c)$ and the σ polarization $(\mathbf{E}\perp c\perp\mathbf{B}, \mathbf{E}\perp\mathbf{B}, \mathbf{k}\|c)$, respectively. The shift and splitting of the exciton lines in the Voigt configuration have not been observed in $(C_{10}H_{21}NH_3)_2PbI_4$.[7] All four absorption lines exhibit essentially the same change. In the π polarization, small high-energy shifts are observed as the magnetic field is increased and the absorption strength shows almost no change. In the σ polarization, the main lines exhibit low-energy shifts and become diminished as the magnetic field is increased. Under higher magnetic fields, subsidiary lines appear on the higher-energy sides and their strength increases with the increase of the magnetic field. Figure 6 shows the peak energies of the first absorption line as a function of the magnetic field. The solid lines are theoretical curves which will be discussed in Sec. IV. As Figs. 5 and 6 show, the main lines shift only slightly for both the π and σ polarizations and the subsidiary line strength is considerably weaker for the σ polarization. This is the reason that no shift and splitting were observed in the Voigt configuration in the previous MA measurement on $(C_{10}H_{21}NH_3)_2PbI_4$,[7] which has a very broad linewidth [$\sim$30 meV full width at half maximum (FWHM)].

IV. DISCUSSION

A. Wannier-exciton model

Within the framework of the effective-mass approximation, the diamagnetic shift exhibits a quadratic field dependence when the effect of the magnetic field is relatively small compared with that of the Coulomb force $(\hbar\omega_c \leq E_b)$, where $\omega_c = eB/\mu$ is the cyclotron frequency and μ is the reduced mass of the exciton.[11-13] On the other hand, if the effect of the magnetic field is much larger than that of the Coulomb energy $(\hbar\omega_c \gg E_b)$, the

diamagnetic shift shows linear dependence on the magnetic field, being governed by the nature of the Landau levels. Since the lowest-energy exciton of $(C_nH_{2n+1}NH_3)_2PbI_4$ has a very large binding energy, its diamagnetic shift observed in MA measurements is expected to obey the quadratic field dependence, reflecting the internal motion of the exciton.

As is well known, the diamagnetic shift of the Wannier exciton depends on the extent of its envelope function, and the diamagnetic coefficient is given by the formula

$$c_0 = \frac{e^2}{8\mu}\langle \phi|x^2+y^2|\phi\rangle \quad \text{for } \mathbf{B}\|\mathbf{z} , \qquad (2)$$

where ϕ is the envelope function of the Wannier-exciton state which describes the relative motion of the electron and hole, μ is the reduced mass of the exciton in the plane perpendicular to the magnetic fields, and e is the electron charge.[14] For the Faraday configuration, $\mathbf{B}$ is taken to be parallel to the c axis of $(C_6H_{13}NH_3)_2PbI_4$. Thus in Eq. (2), the z axis is the c axis and the xy plane is the layer plane.

Since the exciton in $(C_nH_{2n+1}NH_3)_2PbI_4$ is tightly confined in the $[PbI_4]$ layers, which may be as thin as 6.36 Å (which is the distance between the two iodine atoms above and below a Pb^{2+} ion), the relative motion of the electron and hole of the exciton in the well layers is expected to show a strongly two-dimensional character. Therefore, an analysis of the diamagnetic shift in terms of the two-dimensional envelope function may be justified.

The $1s$ 2D envelope function and its binding energy are given by

$$\phi = \left[\frac{2}{\pi(a_B^{(2D)})^2}\right]^{1/2}\exp\left[-\frac{r}{a_B^{(2D)}}\right] , \qquad (3)$$

$$E_b = \frac{e^2}{4\pi\epsilon_0\epsilon_\perp a_B^{(2D)}} , \qquad (4)$$

where

$$a_B^{(2D)} = \frac{2\pi\epsilon_0\epsilon_\perp\hbar^2}{\mu e^2} \qquad (5)$$

is the Bohr radius of the $1s$ 2D exciton, $r = (x^2+y^2)^{1/2}$, and $\epsilon_\perp$ is the effective dielectric constant that the exciton feels. Here we have neglected a small anisotropy in the ab plane of $(C_6H_{13}NH_3)_2PbI_4$. It should be noted that the above 2D Bohr radius is one-half of the three-dimensional (3D) Bohr radius, and the most probable radius a_B^{eff} in the two-dimensional model is $a_B^{(2D)}/2$, that is, $a_B^{(3D)}/4$.[15] Equations (2) and (3) yield the diamagnetic coefficient as

$$c_0 = \frac{e^2}{8\mu}\frac{3}{2}(a_B^{(2D)})^2 . \qquad (6)$$

Putting Eq. (5) into Eq. (6) gives

$$c_0 = \frac{3e^4}{32\pi\epsilon_0\epsilon_\perp\hbar^2}(a_B^{(2D)})^3 . \qquad (7)$$

From the value of c_0 obtained by the MA measurement for the Faraday configuration, we can estimate the 2D

Bohr radius $a_B^{(2D)}$, the most probable radius a_B^{eff}, and the binding energy E_b by use of Eqs. (7) and (4). If the excitons have a typical Wannier character, they should be extended over a number of unit cells. This implies that the exciton radius would be much larger than the well width, 6.36 Å, which is as small as the nearest-neighbor distance of Pb^{2+} ions, 6.24 Å. Then, considering the dielectric-confinement effect, for the dielectric constant $\epsilon_\perp$ we use the high-frequency value averaged over the layers[2,7]

$$\epsilon_\infty = \frac{\epsilon_w L_w + \epsilon_b L_b}{L_w + L_b} , \qquad (8)$$

where ϵ_w and ϵ_b are the high-frequency dielectric constants in the well plane ($[PbI_4]$ layer) and the barrier plane ($[C_6H_{13}NH_3]$ layer), respectively, and L_w ($=6.36$ Å) and L_b ($=9.76$ Å) are the thickness of the well and barrier layers obtained from the x-ray structural analysis. The reason the high-frequency dielectric constants are used is that when the binding energy of the exciton is much larger than the energy of the optical phonons, the relative motion of the electron and hole is too fast for the optical phonons to follow.[10] Since the exact values of ϵ_w and ϵ_b are not available, we tentatively assume the values $\epsilon_w = 6.1$ and $\epsilon_b = 2.1$, which are, respectively, the high-frequency dielectric constants of PbI_2 (Ref. 10) and $[C_nH_{2n+1}NH_3]$.[4] This leads to $\epsilon_\infty = 3.68$.

Table II shows the 2D Bohr radii $a_B^{(2D)}$, the most probable radii a_B^{eff}, and the binding energies E_b estimated as above for the four absorption lines. The 2D Bohr radii of the excitons are comparable with the in-plane lattice constant (≈ 9 Å) of this crystal. Note that it is considerably smaller than the Bohr radius in PbI_2 (~ 20 Å).[10] The value of $a_B^{(2D)}$ is rather insensitive to the choice of the value of $\epsilon_\perp$ because $a_B^{(2D)} \propto \epsilon_\perp^{1/3}$. For example, for the first line $a_B^{(2D)} = 9.5$ Å for $\epsilon_\perp = 3$, $a_B^{(2D)} = 10.1$ Å for $\epsilon_\perp = 3.68$, and $a_B^{(2D)} = 11.2$ Å for $\epsilon_\perp = 5$. Thus we can see that the most probable radius a_B^{eff} (that is, the effective exciton radius) is about 5 Å, which is smaller than the nearest-neighbor distance of Pb^{2+} ions in $(C_6H_{13}NH_3)_2PbI_4$, 6.24 Å. This suggests that the lowest-energy excitons in this crystal may better be described as Frenkel excitons, although in our above analysis we have assumed the existence of a Wannier-exciton-like envelope function. In other words, the exciton theory within the effective-mass approximation may not be a good concept for the lowest-energy excitons in $(C_6H_{13}NH_3)_2PbI_4$. Hence, in Sec. IV B, we will base our analysis on the cationic Frenkel-exciton model.

TABLE II. The 2D Bohr radius $a_B^{(2D)}$, the most probable radius a_B^{eff}, and the binding energy E_b calculated from the diamagnetic coefficient c_0 at each absorption lines.

	First line	Second line	Third line	Fourth line
$a_B^{(2D)}$ (Å)	10.1	9.7	9.2	8.6
a_B^{eff} (Å)	5.1	4.9	4.6	4.3
E_b (meV)	386	402	422	454

B. Cationic Frenkel-exciton model

In the cationic exciton model, the wave function of the exciton is composed of the s and p orbitals of the cation;[16,17] the exciton is considered to involve the transition from the $(ns)^2$ orbitals to the $(ns)(np)$ orbitals of the cation. Earlier studies of excitons in PbI_2 have shown that the exciton state of this crystal, in which Pb^{2+} ions are situated in the centers of quasioctahedra formed by six I^- ions just as in $(C_6H_{13}NH_3)_2PbI_4$ is well described by a cationic exciton model.[16,17] In fact, the reflection spectra of $(C_nH_{2n+1}NH_3)_2PbI_4$ have been interpreted by a similar model.[2]

Since in the cationic Frenkel-exciton model the exciton is considered as an electron-hole pair in which both the electron and the hole are described by wave functions on the "same" cation site, this model should be pertinent to excitons with a strong binding and thus a small radius of relative motion between the electron and hole. In fact, it has been highly successful in understanding the Frenkel-like stacking-fault exciton in BiI_3, which has a very small radius and is localized around the stacking-fault plane.[18] Also, the Zeeman effect of the lowest exciton in PbI_2 has been explained qualitatively but not quantitatively by the cationic Frenkel-exciton model.[19] We expect it should be even more appropriate to $(C_6H_{13}NH_3)_2PbI_4$ than to PbI_2 because, as we have seen in the analysis of the diamagnetic shift, the excitons in $(C_6H_{13}NH_3)_2PbI_4$ have considerably smaller radii than those in PbI_2.

In the cationic Frenkel-exciton model,[16,19] the lowest-exciton states of $(C_6H_{13}NH_3)_2PbI_4$ are composed of the $6s$ and $6p$ orbitals of a Pb^{2+} ion as follows:

$$\phi^1 = \frac{1}{\sqrt{2}}(P_{+e}S_h\beta_e\alpha_h - P_{-e}S_h\alpha_e\beta_h)\cos\theta$$
$$- \frac{1}{\sqrt{2}}P_{0e}S_h(\alpha_e\alpha_h - \beta_e\beta_h)\sin\theta ,$$

$$\phi^2 = \frac{1}{\sqrt{2}}(P_{+e}S_h\beta_e\alpha_h + P_{-e}S_h\alpha_e\beta_h)\cos\theta$$
$$- \frac{1}{\sqrt{2}}P_{0e}S_h(\alpha_e\alpha_h + \beta_e\beta_h)\sin\theta ,$$

$$\phi^3_+ = P_{+e}S_h\beta_e\beta_h\cos\theta - P_{0e}S_h\alpha_e\beta_h\sin\theta ,$$

$$\phi^3_- = P_{-e}S_h\alpha_e\alpha_h\cos\theta - P_{0e}S_h\beta_e\alpha_h\sin\theta ,$$

$$(9)$$

where $S = R_{60}Y_{00}$; $P_0 = R_{61}Y_{10}$; $P_\pm = R_{61}Y_{1\pm1}$; e and h indicate the electron and hole states, respectively; and we have taken the c axis as the z axis, that is $z\|c$. θ is a constant determined by the spin-orbit interaction and the crystal-field splitting as follows:

$$\tan2\theta = \frac{2\sqrt{2}\lambda}{\lambda + 3T}, \quad 0 \le \theta \le \frac{\pi}{2} \tag{10}$$

where

$$\lambda = -\frac{\hbar^2}{4m_e^2}\int \frac{1}{r}\frac{dU}{dr}[R_{61}(r)]^2 r^2 dr ,$$

U is the Coulomb potential,

$$T = \langle P_\pm|H_c|P_\pm\rangle = -\frac{1}{2}\langle P_0|H_c|P_0\rangle ,$$

H_c is the crystal field, and we have taken the tetragonal crystal field as H_c because $(C_6H_{13}NH_3)_2PbI_4$ is almost isotropic in the ab $(=xy)$ plane. From the selection rule and the energy separations between the three peaks in the reflection spectra of $(C_6H_{13}NH_3)_2PbI_4$ single crystals,[20] we estimate that $T = -0.505$ eV and $\lambda = -0.322$ eV, and hence $\sin\theta = 0.227$. The corresponding energies of each state in Eq. (9) are

$$E_1 = E_A - v \quad \text{for } \phi^1 ,$$

$$E_2 = E_A - v + 2w\sin^2\theta \quad \text{for } \phi^2 , \tag{11}$$

$$E_3 = E_A - v + w\cos^2\theta \quad \text{for } \phi^3_+, \phi^3_- ,$$

where v is the Coulomb integral and w is the exchange integral,

$$v = \langle P_iS|v(r-r')|P_iS\rangle ,$$

$$w = \langle P_iS|v(r-r')|SP_i\rangle \quad (i = +, 0, -) ,$$

$v(r-r')$ is the Coulomb potential between the electron and hole, E_A is the energy between the $6s$ states and the lowest $6p$ states of a Pb^{2+} ion, and the long-range exchange interaction has been neglected. The selection rule for the optical transition to each state is easily obtained from Eq. (9):

$$\phi^1: \quad \text{forbidden} ,$$

$$\phi^2: \quad \mathbf{E}\|\mathbf{z} , \tag{12}$$

$$\phi^3_\pm: \quad \mathbf{E}\|\mathbf{x}, \mathbf{y} .$$

Now that the lowest exciton states have been determined as above, we can analyze the effect of the magnetic field on the lowest exciton states. The magnetic-field effect for this model is described by the Zeeman-term Hamiltonian

$$H_B = \frac{\mu_B}{\hbar}(l_e + g_e s_e)\cdot\mathbf{B} - \frac{\mu_B}{\hbar}(l_h + g_h s_h)\cdot\mathbf{B} , \tag{13}$$

where l_e, g_e, s_e are the orbital momentum, the g factor, and the spin momentum of the electron, and l_h, g_h, s_h are those of the hole.

(1) *Faraday configuration* $(\mathbf{B}\|c, \mathbf{E}\perp c, \mathbf{k}\|c)$. From Eqs. (9), (11), (13), and $\mathbf{B} = (0, 0, B)$, the matrix for the total Hamiltonian which includes H_B of the lowest exciton is given by

$$
\begin{array}{cccc}
\phi^1 & \phi^2 & \phi^3_+ & \phi^3_-
\end{array}
$$
$$
\begin{bmatrix}
E_1 & \gamma B & 0 & 0 \\
\gamma B & E_2 & 0 & 0 \\
0 & 0 & E_3 + \delta B & 0 \\
0 & 0 & 0 & E_3 - \delta B
\end{bmatrix}, \tag{14}
$$

where

$$\gamma = \mu_B[\cos^2\theta - \tfrac{1}{2}g_e(\cos^2\theta - \sin^2\theta) - \tfrac{1}{2}g_h] ,$$

$$\delta = \mu_B[\cos^2\theta - \tfrac{1}{2}g_e(\cos^2\theta - \sin^2\theta) + \tfrac{1}{2}g_h] \tag{15}$$

$$(> 0 \text{ in general}) .$$

Then, the eigenwave functions ϕ_{Farad} and the corresponding eigenenergies E_{Farad} are

$$\phi_{\mathrm{Farad}}^{1,2}=a_{1,2}\phi^1+b_{1,2}\phi^2 \ ,$$

$$\phi_{\mathrm{Farad}}^{3,4}=\phi_{\pm}^3 \ , \tag{16}$$

$$E_{\mathrm{Farad}}^{1,2}=\tfrac{1}{2}\{E_1+E_2\pm[(E_1-E_2)^2+4\gamma^2B^2]^{1/2}\} \ ,$$

$$E_{\mathrm{Farad}}^{3,4}=E_3\pm\delta B \ , \tag{17}$$

where

$$a_{1,2}=\frac{\gamma B}{[(E_1-E_{\mathrm{Farad}}^{1,2})^2+\gamma^2B^2]^{1/2}} \ ,$$

$$b_{1,2}=\frac{E_{\mathrm{Farad}}^{1,2}-E_1}{[(E_1-E_{\mathrm{Farad}}^{1,2})^2+\gamma^2B^2]^{1/2}} \ .$$

Thus, the selection rule for the optical transition in the Faraday configuration is

$$\phi_{\mathrm{Farad}}^{1,2}: \quad \mathbf{E}\|\mathbf{z} \ (\text{not observable}) \ ,$$

$$\phi_{\mathrm{Farad}}^{3}: \quad \sigma^+ \ \text{polarization or} \ \mathbf{E}\|\mathbf{x},\mathbf{y} \ , \tag{18}$$

$$\phi_{\mathrm{Farad}}^{4}: \quad \sigma^- \ \text{polarization or} \ \mathbf{E}\|\mathbf{x},\mathbf{y} \ .$$

Equations (17) and (18) describes the Zeeman splitting in the Faraday configuration for the σ^+ and σ^- polarizations.

We assume $E_2-E_3=0.004$ eV as the only adjustable parameter which is close to the value 0.0047 eV, obtained from the Kramers-Kronig analysis of the polarized reflection spectra for $(C_{10}H_{21}NH_3)_2PbI_4$.[20] This data together with Eq. (11) allows us to calculate all the parameters needed. For the first absorption line $(E_3=2.341\,35$ eV) of our MA measurement, the results are

$$E_1=2.340\,85 \ \text{eV} \ ,$$

$$E_2=2.345\,35 \ \text{eV} \ , \tag{19}$$

$$E_3=2.341\,35 \ \text{eV} \ .$$

Using the atomic g factor where $g_e=g_h=2$ (which is valid for the cationic Frenkel exciton), Eqs. (15) and (17), the effective g factor for the Zeeman splitting is calculated as

$$g_{\mathrm{eff}}=\frac{2\delta}{\mu_B}=2(1+\sin^2\theta)=2.10 \ , \tag{20}$$

which is rather close to the effective g factor $g_\perp$ obtained from our MA measurement [1.80 (Table I)]. It should be noted that the experimental $g_\perp$ value for PbI_2, 0.89, is much smaller than the theoretical value, 2.23.[10,19] This suggests that the present model is even more valid for $(C_6H_{13}NH_3)_2PbI_4$ than for PbI_2. This is consistent with the fact that the lowest exciton in $(C_6H_{13}NH_3)_2PbI_4$ has a much larger binding energy and a much smaller radius than that in PbI_2.

(2) Voigt configuration $(\mathbf{B}\perp c, \mathbf{E}\perp c, \mathbf{k}\|c)$. From Eqs. (9), (11), and (13) and $\mathbf{B}=(B,0,0)$, the matrix of the total Hamiltonian for the lowest exciton is given by

$$\begin{array}{cccc} \phi^1 & \phi^2 & \phi_+^3 & \phi_-^3 \end{array}$$

$$\begin{bmatrix} E_1 & 0 & -\zeta B & \zeta B \\ 0 & E_2 & \eta B & \eta B \\ -\zeta B & \eta\beta & E_3 & 0 \\ \zeta B & \eta\beta & 0 & E_3 \end{bmatrix} , \tag{21}$$

where

$$\zeta=\mu_B\left[-\sin\theta\cos\theta+\frac{1}{2\sqrt{2}}g_e\sin^2\theta+\frac{1}{2\sqrt{2}}g_h\right] \ ,$$

$$\eta=\mu_B\left[-\sin\theta\cos\theta+\frac{1}{2\sqrt{2}}g_e\sin^2\theta-\frac{1}{2\sqrt{2}}g_h\right] \ . \tag{22}$$

The eigenfunctions ϕ_{Voigt} and the corresponding eigenergies E_{Voigt} are calculated from Eq. (21) as follows:

$$\phi_{\mathrm{Voigt}}^{1,2}=c_{1,2}\phi^1+d_{1,2}(\phi_+^3-\phi_-^3) \ ,$$

$$\phi_{\mathrm{Voigt}}^{3,4}=c_{3,4}\phi^2+d_{3,4}(\phi_+^3+\phi_-^3) \ , \tag{23}$$

$$E_{\mathrm{Voigt}}^{1,2}=\tfrac{1}{2}\{(E_1+E_3)\pm[(E_1-E_3)^2+8\zeta^2B^2]^{1/2}\} \ ,$$

$$E_{\mathrm{Voigt}}^{3,4}=\tfrac{1}{2}[(E_2+E_3)\pm[(E_2-E_3)^2+8\eta^2B^2]^{1/2}\} \ , \tag{24}$$

where

$$c_{1,2}=\frac{2\zeta B}{[2(E_{\mathrm{Voigt}}^{1,2}-E_1)^2+4\zeta^2B^2]^{1/2}} \ ,$$

$$d_{1,2}=\frac{E_1-E_{\mathrm{Voigt}}^{1,2}}{[2(E_{\mathrm{Voigt}}^{1,2}-E_1)^2+4\zeta^2B^2]^{1/2}} \ ,$$

$$c_{3,4}=\frac{2\eta B}{[2(E_{\mathrm{Voigt}}^{3,4}-E_2)^2+4\eta^2B^2]^{1/2}} \ , \tag{25}$$

$$d_{3,4}=\frac{E_{\mathrm{Voigt}}^{3,4}-E_2}{[2(E_{\mathrm{Voigt}}^{3,4}-E_2)^2+4\eta^2B^2]^{1/2}} \ .$$

According to Eqs. (9) and (23), the selection rule for the optical transition in the Voigt configuration is given by

$$\phi_{\mathrm{Voigt}}^{1,2}: \quad \mathbf{E}\|\mathbf{x} \ (\pi \ \text{polarization}) \ ,$$

$$\phi_{\mathrm{Voigt}}^{3,4}: \quad \mathbf{E}\|\mathbf{y} \ (\sigma \ \text{polarization}) \tag{26}$$

$$\text{or} \ \mathbf{E}\|\mathbf{z} \ (\text{not observable}) \ .$$

Figure 6 shows the experimental shifts and splittings and the theoretical curves calculated from Eqs. (19), (22), and (24) and $g_e=g_h=2$ for the first absorption line. In the theoretical curves, the upper and lower lines for the π polarization correspond to the ϕ_{Voigt}^1 and ϕ_{Voigt}^2 states, respectively, while the upper and lower lines for the σ polarization correspond to the ϕ_{Voigt}^3 and ϕ_{Voigt}^4 states, respectively. Figure 7 shows the relative values of the absorption strength of the main line (upper line in Fig. 6) and the subsidiary line (lower line in Fig. 6) for the π polarization calculated from Eqs. (19), (22), (23), (24), and (25) and $g_e=g_h=2$ for the first absorption line. Figure 8 shows the relative values of the absorption strength of the main line (lower line in Fig. 6) and subsidiary line (upper line in Fig. 6) for the σ polarization calculated from Eqs.
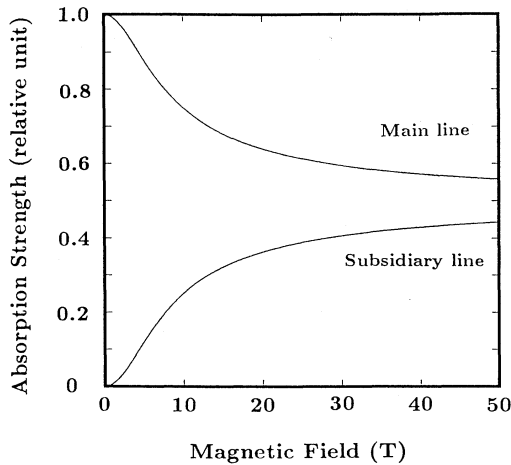
FIG. 7. Relative absorption strength of the main and subsidiary lines for the π polarization calculated for the first absorption line.

FIG. 8. Relative absorption strength of the main and subsidiary lines for the σ polarization calculated for the first absorption line. Open circles are the experimental results for the main line.

(19), (22), (23), (24), and (25) and $g_e = g_h = 2$ with the experimental results for the first absorption line. Because of the ambiguity in determining the absorption strength of the subsidiary lines, the experimental results for those lines are not shown.

For the σ polarization, the experimental results fit the theoretical curves very well. In Fig. 6, the energy positions of the main and subsidiary lines show very good agreement between experiment and theory. Furthermore, in Figs. 5 and 8, the absorption strength of the main and subsidiary lines shows semiquantitative agreement between experiment and theory. For the π polarization, the experimental result only shows small upward shifts. We believe that this is due to the overlap of the lower and upper lines displayed in Fig. 6, whose energy separation is much smaller than the widths of the absorption lines. This is confirmed by computing the overlap of the two separate Lorentzian lines, each 10 meV wide, whose relative intensities are given in Fig. 7. Thus, the MA spectra of $(C_6H_{13}NH_3)_2PbI_4$ in the Voigt configuration have been semiquantitatively interpreted by the cationic Frenkel-exciton model. This result is compatible with the extremely large oscillator strength and binding energy of the exciton in this material. The binding energy of the exciton should be interpreted in terms of the site shift energy due to the dipole-dipole interactions as the zeroth-order approximation.

The diamagnetic shift, though very small, has clearly been observed experimentally in the Faraday configuration, while it has not been detected in the Voigt configuration. This gives some clue as to the internal motion of the exciton in this material; the excitons have some, though very small, 2D-like spatial extent in the
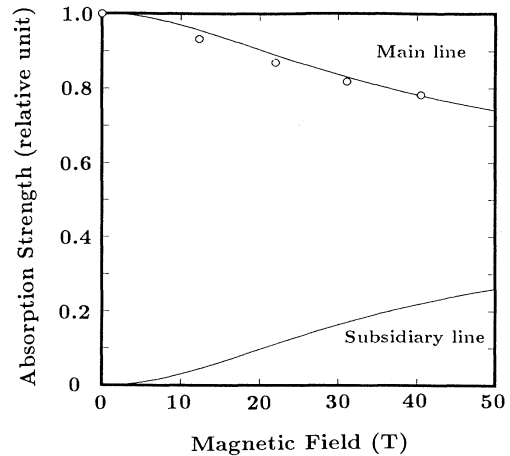
well plane, which may be taken into account by considering charge transfer (CT) –exciton-like states, in which the electrons are transferred to the nearest neighbor Pb^{2+} ions, as perturbations to the cationic Frenkel-exciton model.

V. CONCLUSION

Magnetoabsorption spectra of the lowest-energy exciton in $(C_6H_{13}NH_3)_2PbI_4$ have been measured for the Faraday and Voigt configurations under magnetic fields up to 42 T at 4.2 K. The diamagnetic coefficient obtained is much smaller than that of PbI_2 and both energy shifts and splittings of the MA spectra are explained in terms of the cationic Frenkel-exciton model. This indicates that the lowest excitons in $(C_6H_{13}NH_3)_2PbI_4$ have a strong Frenkel-exciton character; as the zeroth-order approximations, the Frenkel-exciton model is more valid compared with the Wannier-exciton model based on the effective-mass approximation in this excitonic system probably because of its unique two-dimensional structure.

[1] T. Ishihara, J. Takahashi, and T. Goto, Solid State Commun. **69**, 933 (1989).
[2] T. Ishihara, J. Takahashi, and T. Goto, Phys. Rev. B **42**, 11 099 (1990).
[3] C. Q. Xu, Ph.D. thesis, The University of Tokyo, 1991.
[4] C. Q. Xu, S. Fukuta, H. Sakakura, T. Kondo, S. Takeyama, N. Miura, K. Kumata, Y. Takahashi and R. Ito (unpublished).
[5] L. V. Keldysh, Pis'ma Zh. Eksp. Teor. Fiz. **29**, 716 (1979)

[JETP Lett. **29**, 658 (1979)].

[6]E. Hanamura, N. Nagaosa, M. Kumagai, and T. Takagahara, J. Material. Sci. Eng. **1**, 255 (1988).

[7]C. Q. Xu, H. Sakakura, T. Kondo, S. Takeyama, N. Miura, Y. Takahashi, K. Kumata, and R. Ito, Solid State Commun. **79**, 249 (1991).

[8]S. Takeyama, K. Watanabe, N. Miura, T. Komatsu, K. Koike, and Y. Kaifu, Phys. Rev. B **41**, 4512 (1990).

[9]N. Miura, T. Goto, K. Nakao, S. Takeyama, T. Sakakibara, and F. Herlach, J. Magn. Magn. Mater. **54-57**, 1409 (1986).

[10]Y. Nagamune, S. Takeyama, and N. Miura, Phys. Rev. B **40**, 8099 (1989).

[11]H. Q. Hon, W. Staguhn, N. Miura, Y. Segawa, S. Takeyama, Y. Aoyagi, and J. M. Zhou, Solid State Commun. **74**, 687 (1990).

[12]W. Ossau, B. Jakel, E. Bangert, G. Landwehr, and G. Weimann, Surf. Sci. **174**, 188 (1986).

[13]S. Tarucha, H. Iwamura, T. Saku, H. Okamoto, Y. Iwasa, and N. Miura, Surf. Sci. **174**, 194 (1986).

[14]R. S. Knox, in *Solid State Physics: Theory of Excitons*, edited by F. Seitz and D. Turnbull (Academic, New York, 1963), Suppl. 5, p. 79.

[15]D. S. Chemla and D. A. B. Miller, J. Opt. Soc. Am. B **2**, 1155 (1985).

[16]I. Ch. Schlüter and M. Schlüter, Phys. Rev. B **9**, 1652 (1974).

[17]G. Harbeke and E. Tosatti, Phys. Rev. Lett. **28**, 1567 (1972).

[18]T. Komatsu, Y. Kaifu, S. Takeyama, and N. Miura, Phys. Rev. Lett. **58**, 2259 (1987).

[19]Y. Nagamune, S. Takeyama, and N. Miura, Phys. Rev. B **43**, 12 401 (1991).

[20]J. Takahashi (unpublished).